Title

Lead-Free Organic—Perovskite Hybrid Quantum Wells for Highly Stable Light-Emitting Diodes

Journal

ACS Nano, 15(4)

ISSN

1936-0851

Authors

Wang, Kang

Jin, Linrui

Gao, Yao

et al.

Publication Date

2021-04-27

DOI

10.1021/acsnano.1c00872

Lead-Free Organic-Perovskite Hybrid Quantum Wells for Highly Stable Light-Emitting Diodes

*Kang Wang‡, Linrui Jin‡, Yao Gao, Aihui Liang, Blake P. Finkenauer, Wenchao Zhao, Zitang Wei, Chenhui Zhu, Tzung-Fang Guo, Libai Huang, Letian Dou**

KEYWORDS: lead-free perovskites, hybrid quantum wells, semiconducting organic cations, charge injection, energy transfer, light-emitting diodes.

ABSTRACT: Two-dimensional perovskites that could be regarded as natural organic-inorganic hybrid quantum wells (HQWs) are promising for light-emitting diodes (LEDs) applications. High photoluminescence quantum efficiencies (approaching 80%) and extremely narrow emission bandwidth (less than 20 nm) have been demonstrated in their single crystals; however, a reliable electrically-driven LED device has not been realized owing to inefficient charge injection and extremely poor stability. Furthermore, the use of toxic lead raises concerns. Here, we report novel Sn(II)-based organic-perovskite hybrid quantum wells (HQWs) employing molecularly tailored organic semiconducting barrier layers for efficient and stable LEDs. Utilizing femtosecond transient absorption spectroscopy, we demonstrate the energy transfer from organic barrier to inorganic perovskite emitter occurs faster than the intramolecular charge transfer in the organic layer. Consequently, this process allows efficient conversion of lower-energy emission associated with the organic layer into higher-energy emission from the perovskite layer. This greatly broadened the candidate pool for the organic layer. Incorporating a bulky small bandgap organic barrier in the HQW, charge transport is enhanced and ion migration is greatly suppressed. We demonstrate a HQW-LED device with pure red emission, a maximum luminance of 3466 cd m^{-2}, a peak external quantum efficiency (EQE) up to 3.33%, as well as a

remarkable operational stability over 150 hours, which are significantly better than previously reported lead-free perovskite LEDs.

Quantum wells formed from thin layers of semiconductor well surrounded by barrier materials are useful in various optoelectronic devices ranging from LEDs, lasers, to thermoelectrics as well as photodetectors.[1-4] Compared with III-V quantum wells, which are fabricated by expensive chemical vapor deposition or molecular beam epitaxy processes, two-dimensional (2D) halide perovskites with one inorganic layer sandwiched by two organic cations layers can be easily assembled from solution under mild conditions. These hybrid quantum wells (HQWs) are promising for LED applications owing to remarkable structure and composition tunability and excellent optoelectronic properties.[5-12] For instance, a high solid-state photoluminescence quantum efficiency approaching 80% and an extremely narrow emission bandwidth of ~20 nm have been demonstrated in typical $(PEA)_2PbBr_4$ HQW, where PEA is phenylethylammonium.[13] Despite the promising optical properties of these HQW configurations, their LED device performance[14-18] lags far behind conventional 3D[19-24] or 2D/3D[25-33] mixed halide perovskites, regarding both efficiency and stability; and the reasons for the low device performance are still largely unknown.

We hypothesize that the commonly used short and insulating organic cations (such as butylammonium, BA^+ and PEA^+) set a high energy barrier for charge carrier injection and meanwhile they are not effective enough in blocking ion migration between the perovskite layers under an electrical bias. To tackle the abovementioned fundamental issues, we explore a material design strategy by incorporating bulky and rigid semiconducting organic cations into the 2D perovskite lattice to spontaneously decrease the quantum well energy barrier height and suppress the ion migration.[34-35] Herein, we report a novel lead-free HQW 2D crystal based on a conjugated organic cation, 7-(thiophen-2-yl)benzothiadiazol-4-yl)-[2,2'-bithiophen]-5-yl)ethylammonium

iodide (BTmI). This molecular engineering approach leads to strongly confined 2D HQWs with type-I alignment that features improved charge transport property and enhanced stability. Moreover, the ultrafast energy transfer from organic layer to perovskite layer in this HQW ensures rapid carrier injection into the perovskite wells with reduced non-radiative losses associated with the states above the final emissive species. On this basis, we demonstrate pure red Sn(II)-based HQW-LEDs reaching a luminance of 3466 cd m^{-2}, peak EQE of 3.33%, as well as high color purity with Commission Internationale de l'Eclairage (CIE) coordinates of (0.69, 0.31). Importantly, our LEDs show excellent operational stability approaching 10^4 minutes (>150 hours) lifetime at an initial luminance of 40 cd m^{-2}, which is comparable to the highly stable Pb(II)-perovskite LEDs.[22, 36-37] These discoveries not only provide important fundamental insights on the organic-perovskite interactions, but also afford us a novel and stable materials platform for solid-state lighting and displays.

RESULTS AND DISCUSSION

Single Crystal Structure and Band Alignment. Figure 1a and 1b show the crystal structure of $(BTm)_2SnI_4$ along *b*-axis and *a*-axis, respectively, where a single inorganic $[SnI_4]^{2-}$ slab is sandwiched between two layers of organic cation (BTm^+) spacers, which can be considered as an organic-inorganic HQW with inorganic octahedrons acting as the quantum well and the organic cations as the energy barrier. The $(BTm)_2SnI_4$ single crystal belongs to *P*-1 space group with a = 12.073 Å, b = 12.175 Å, c = 34.588 Å, α = 84.96°, β = 83.24°, and γ = 89.99° (Table S1 for more details). Specifically, the Sn-I-Sn bond angles in $(BTm)_2SnI_4$ single-crystal structures are relatively smaller and Sn-I bonds lengths are slightly shorter (Figure 1c) compared with the PEA^+ based Sn-perovskite isomorphism,[38] implying the formation of more contracted in-plane crystal

lattice with enhanced intrinsic stability. As displayed in Figure 1d, $(BTm)_2SnI_4$ thin film shows a sharp excitonic absorption peak at 615 nm (corresponding to 2.01 eV), while pure BTm^+ cation film shows an absorption onset at 590 nm (2.10 eV). The photoluminescence (PL) emission of $(BTm)_2SnI_4$ HQWs ranging from 600 nm to 700 nm clearly originates from the inorganic $[SnI_4]^{2-}$ layer,[38] in which the absence of PL from organic molecule BTm^+ can be ascribed to the complete energy transfer from organic barriers to inorganic wells. Meanwhile, the excitation spectrum of $(BTm)_2SnI_4$ thin film displays obvious peaks between 300 - 400 nm (Figure S1), which is different from the absorption of $(PEA)_2SnI_4$ sample, but coincident with the absorption of BTm^+. This, again, undoubtedly verifies the energy transfer from BTm^+ cations to $[SnI_4]^{2-}$ perovskites. These optical absorption and PL results suggest the formation of a type-I HQW configuration in $(BTm)_2SnI_4$ (Figure 1e), which could facilitate exciton confinement in $[SnI_4]^{2-}$ octahedron layers for radiative recombination, making the HQWs efficient light-emitters (PLQY = 7.5 ± 0.3%, Figure S2)

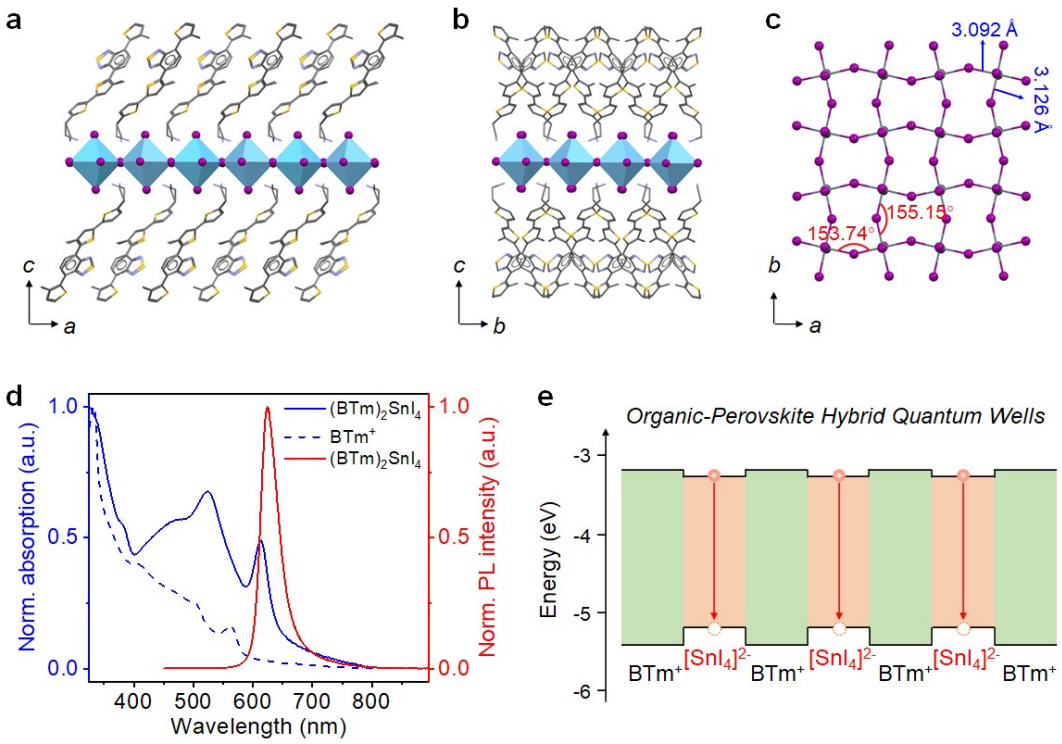

Figure 1. Two-dimensional organic-perovskite hybrid quantum well. (a - b) Side view of the quantum-well-like single crystal structure of a $(BTm)_2SnI_4$ sheet along *b* axis (a) and *a* axis (b). (c) Plan view of a single inorganic layer in $(BTm)_2SnI_4$ with grey for carbon atom, blue for nitrogen atom, yellow for sulfur atom, purple for iodine atom, and cyan diamonds for $[SnI_6]^{4-}$ octahedrons. (d) UV-vis and PL spectra of BTm^+ cation and $(BTm)_2SnI_4$ polycrystalline films. (e) Schematic of relative band alignment of organic (BTm^+) and inorganic ($[SnI_4]^{2-}$) layers within 2D hybrid perovskites. The red arrows indicate the radiative recombination of confined excitons in such 2D HQWs.

Energy Transfer Process and Proposed Emission Mechanism. PL and electroluminescence (EL) studies were then conducted to investigate the energy transfer process in this 2D HQW materials. We compare the results from $(BTm)_2SnI_4$ to those from lead-based 2D perovskites, $(BTm)_2PbI_4$. Figure S3 illustrates the single crystal structure of $(BTm)_2PbI_4$, which shows the similar HQW structure to $(BTm)_2SnI_4$. It has been reported that $(BTm)_2PbI_4$ exhibits an inverted type-I alignment with inorganic $[PbI_4]^{2-}$ perovskites serving as donor and organic BTm^+ as

acceptor, which give rise to broad PL and EL emission from BTm^+ ranging from 540 to 820 nm (Figure 2a and 2b).[34] Owing to its donor-acceptor feature and solvent-polarity-dependent emission of BTm^+ molecule (see Figure S4 and related discussions), the broad emission peaked at 653 nm (1.90 eV) could be ascribed to a lower-energy intramolecular charge-transfer (ICT) state.[39] In comparison, interestingly, both PL and EL of $(BTm)_2SnI_4$ thin film feature higher-energy emission at 627 nm (1.97 eV) from the inorganic $[SnI_4]^{2-}$ layer without the lower-energy (ICT) emission from the organic layer (Figure 2a and 2b). Note, the BTm^+ molecule exhibits exactly the same conformations in both types of HQWs [see Figure 1a for the structure of $(BTm)_2SnI_4$ and Figure S3 for structure of $(BTm)_2PbI_4$]. Therefore, in principle, BTm^+ should emit similarly in both lead-iodide and tin-iodide matrices. The PL quenching from organic layers in $(BTm)_2SnI_4$ indicates the energy transfer from BTm^+ to $[SnI_4]^{2-}$ exceeds intramolecular charge-transfer and vibrational relaxation within the BTm^+ molecules. Based on this result, we propose an energy diagram of exciton evolution in our HQW systems (Figure 2c). In $(BTm)_2PbI_4$, BTm^+ can be excited to the high-level local excitation (LE) state and then relax to its low-lying ICT state, leading to broad low-energy emission (no energy transfer to the $[PbI_4]^{2-}$ layer due to large energy mismatch). By contrast, in $(BTm)_2SnI_4$, BTm^+ absorbs excitation energy to LE state. Before these excitons relax to ICT state through vibrational relaxation, they undergo energy transfer to $[SnI_4]^{2-}$ perovskite layers, which leads to higher-energy emission from inorganic layer with the absence of lower-energy emission from organic layer. These observations suggest that the energy transfer between BTm^+ and $[SnI_4]^{2-}$ needs to be much faster than the transition from LE to ICT.

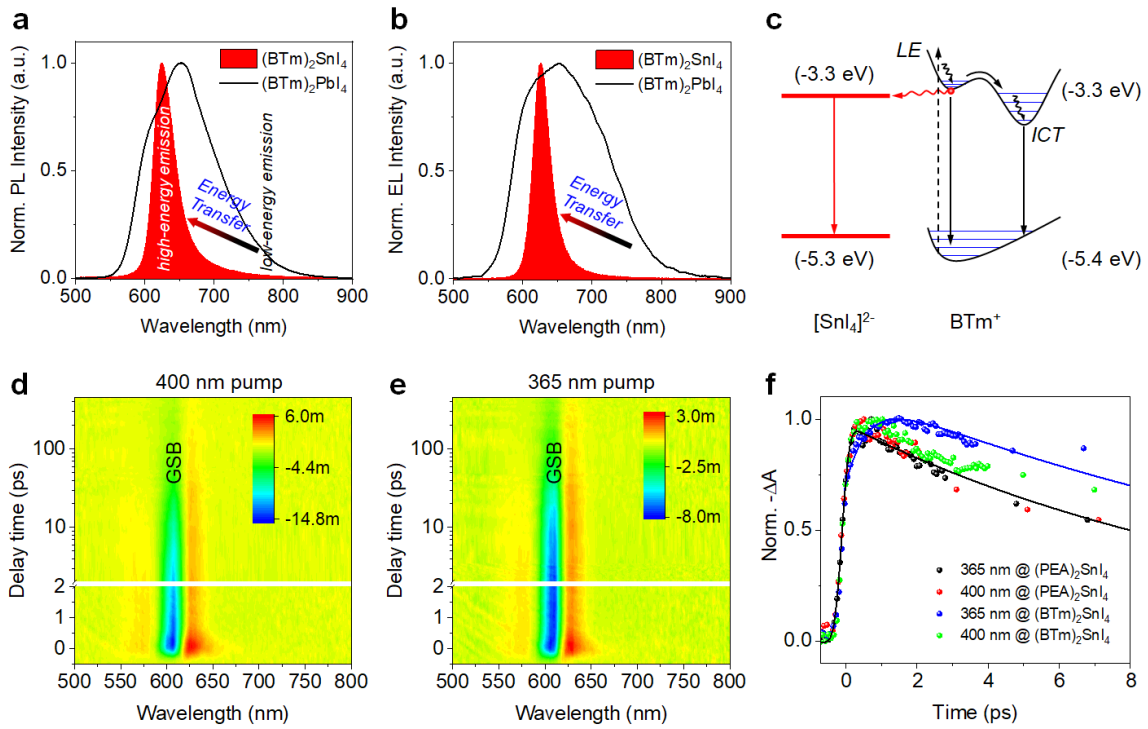

Figure 2. Photo-physics and proposed emission mechanism in organic-perovskite HQWs. (a) PL and (b) EL spectra of 2D organic-perovskite HQW thin films with different inorganic contents. The arrows indicate the energy conversion of low-energy emission associate with organic cations into high-energy emission from inorganic perovskites via energy transfer. (c) Schematic illustration of relative energy alignment in $(BTm)_2SnI_4$ hybrid perovskites. (d - e) Pseudo-color maps of transient absorption spectra of (BTm)2SnI4 thin films pumped at 400 nm (d) and 365 nm (e). (f) Normalized kinetic traces at corresponding bleaching wavelengths for $(BTm)_2SnI_4$ and $(PEA)_2SnI_4$ HQW films with different excitation wavelengths. The TA dynamics of $(PEA)_2SnI_4$ control sample was fitted by a single exponential decay function (black curve). And the TA dynamics of $(BTm)_2SnI_4$ sample with 365 nm excitation was fitted with an energy transfer model (blue curve).

To directly measure the energy transfer rate, femtosecond transient absorption (TA) measurements were then conducted on $(BTm)_2SnI_4$ and $(PEA)_2SnI_4$ thin films with different excitation wavelengths (400 nm and 365 nm), and probed in 500 - 800 nm. Figure 2d and 2e exhibited pseudo-color maps of TA spectra for $(BTm)_2SnI_4$. The results from a control sample

$(PEA)_2SnI_4$ are presented in Figure S5, where the PEA^+ was not excited and thus no energy transfer is expected. Distinct ground-state bleach (GSB) peaks centered at 605 nm for $(BTm)_2SnI_4$ and 600 nm for $(PEA)_2SnI_4$ were observed in these 2D HQWs, which are in agreements with their steady-state absorption spectra. The normalized -ΔA against delay time for GSB of both samples are plotted in Figure 2f. Since only inorganic $[SnI_4]^{2-}$ layer in $(PEA)_2SnI_4$ HQWs can be excited with both 365 nm and 400 nm pump laser, the GSB signal in $(PEA)_2SnI_4$ shows almost identical dynamics under different excitation wavelengths (black and red dots in Figure 2f). For $(BTm)_2SnI_4$, the dynamics by 400 nm and 365 nm pump are significantly different. With a pump wavelength of 365 nm, the kinetics of $(BTm)_2SnI_4$ rises in ~1 ps and decays much slower (blue dots in Figure 2f) than $(PEA)_2SnI_4$. Because most of the pump wavelength of 365 nm was absorbed by organic cations, the rise time observed reflects the energy transfer from BTm^+ to $[SnI_4]^{2-}$. With a 400 nm pump, both BTm^+ and $[SnI_4]^{2-}$ can be excited (see the absorption spectra of BTm^+ and $(BTm)_2SnI_4$ in Figure 1d), and a slightly increased decay time in the GSB kinetics (green dots in Figure 2f) is observed compared to those of $(PEA)_2SnI_4$ sample. By fitting the 365 nm pumped dynamics in $(BTm)_2SnI_4$ using the model detailed in Methods in the Supporting Information, we extracted the energy transfer time constant from BTm^+ to $[SnI_4]^{2-}$ to be ~0.6 ps. Because LE to ICT conversion usually takes place in several picoseconds,[40] the energy transfer outcompetes the transition from LE to ICT in $(BTm)_2SnI_4$, which leads to completely quenched emission from BTm^+ cation and intense emission from $[SnI_4]^{2-}$ perovskite. This ultrafast energy transfer can also ensure rapid carrier injection into the inorganic perovskite wells with reduced non-radiative losses associated with the states above the final emissive species.

Device Characteristics. To investigate the effects of conjugated organic cation design on device performance, we incorporated HQWs in LEDs with a device structure of glass/ITO/m-PEDOT:PSS/HQWs/TPBi/LiF/Al (Figure 3a), where m-PEDOT:PSS is short for PSS-Na doped PEDOT:PSS,[41] TPBi is the abbreviation of 1,3,5-tris(1-phenyl-1H-benzimidazol-2-yl)benzene, HQWs represent 2D $(BTm)_2SnI_4$ organic-perovskite hybrid thin films, and ITO is indium tin oxide. Figure 3b presents the cross-section scanning electron microscopy (SEM) image of a working device, where a multilayered structure is clearly observed. Essentially, the thicknesses of m-PEDOT:PSS, HQWs, TPBi can be determined to be around 40, 25, 80 nm, respectively. The SEM image (Figure 3c) shows a uniform HQWs film with a complete surface coverage, which is essentially free of pinholes. Atomic force microscope (AFM) image exhibits a roughness of 1.71 nm (root-mean-square, r.m.s.) for the as-prepared HQW film (Figure 3d), which can be beneficial to reduce current leakage in devices. The crystal structure of the HQW thin film was further examined by grazing incidence wide-angle X-ray scattering (GIWAXS, Figure 3e), where a series of intense spots were noticed along q_z direction, suggesting that the HQW thin film is highly oriented. This further indicates that the alternating BTm^+ cation layers and $[SnI_4]^{2-}$ perovskites are paralleled to the substrate, similar to conventional III-V semiconductor quantum wells. On this basis, the distance between adjacent perovskite octahedral layers was evaluated to be 33.9 Å, which is identical with its single crystal data. Importantly, this "face-on" orientation is expected to block the ion migration in the vertical direction effectively when a large voltage is applied during device operation. This is fundamentally different from previous works including vertically-aligned quasi-2D perovskites in devices, where ion migration is inevitable. Figure 3f displays the EL spectra of HQW-LED under varied driving voltages with an EL image shown in

its inset. Those spectra centered at 627 nm with a narrow full-width at half-maximum (FWHM) of 27.8 nm (~85 meV) corresponding to the CIE chromaticity coordinates at (0.69, 0.31) (inset of Figure 3f), suggesting a high color-purity red emission. This FWHM is even smaller than that in perovskite quantum dots red LEDs,[42] which is appealing for high-definition displays. The central wavelength of the EL spectra doesn't shift with increased the driving voltage, indicating the improved color stability of our HQW-LED. Figure 3g exhibits the current density-voltage-luminance (*J*-*V*-*L*) curves of our champion HQW-LED device, in which the maximum luminance of 3466 cd m^{-2} was achieved at 13.2 V. Meanwhile, the EQE up to 3.33% was obtained at a luminance of 15 cd m^{-2} (Figure 3h), which exceeds those Pb or Sn based HQW-LEDs (Table S2).[43-49] The film optimization based on different anti-solvent treatment and corresponding device characterizations can be found in Figure S6-S8. In addition, we can fabricate larger area devices, which also exhibit similar brightness and device efficiency (see Figure S9 and Table S3).

To further study the role of cation design in charge injection, we employed additional π-conjugated organic barriers with different band alignments relative to $[SnI_4]^{2-}$ well, including PEA^+, thiophenylethylammonium ($1T^+$), bithiophenylethylammonium ($2T^+$), and quaterthiophenylethylammonium ($4Tm^+$), to fabricate Sn-based HQW-LEDs. The chemical structures and band alignments of all cations in this study are listed in Figure S10. The optical properties and structural characterizations of these HQW thin films are shown in Figure S11. The EQE distributions for HQW-LEDs with different cations are presented in Figure 3i, which shows gradually increased efficiency from 0.15 ± 0.06% for PEA^+ to 2.96 ± 0.20% for BTm^+. This trend agrees well with the decrease of the lowest unoccupied molecular orbital (LUMO) level and increase of highest occupied molecular orbital (HOMO) of organic cations, which benefit charge

transport from organic semiconducting barrier to inorganic perovskite well[50] (also see single-carrier device results in Figure S12) and lead to enhanced luminance and EQE. The *J-V-L*, EQE, and EL spectra of the champion devices for PEA^+, $1T^+$, $2T^+$, and $4Tm^+$ are summarized in Figure S13. Generally, the vacancies or defects are critical in limiting the devices performance of perovskite LEDs.[51-52] To further boost the Sn-based HQW device performance, more strategies could be adopted to passivate the Sn^{2+} vacancies or defects and suppress the oxidization of Sn^{2+}, such as the introduction of naphthol sulfonic salt,[45] H_3PO_2,[46] phenylhydrazine hydrochloride,[48] valeric acid,[49] SnX_2,[53] tin powder,[54] $SnCl_2$ with sulfonic salt,[55], *etc*.

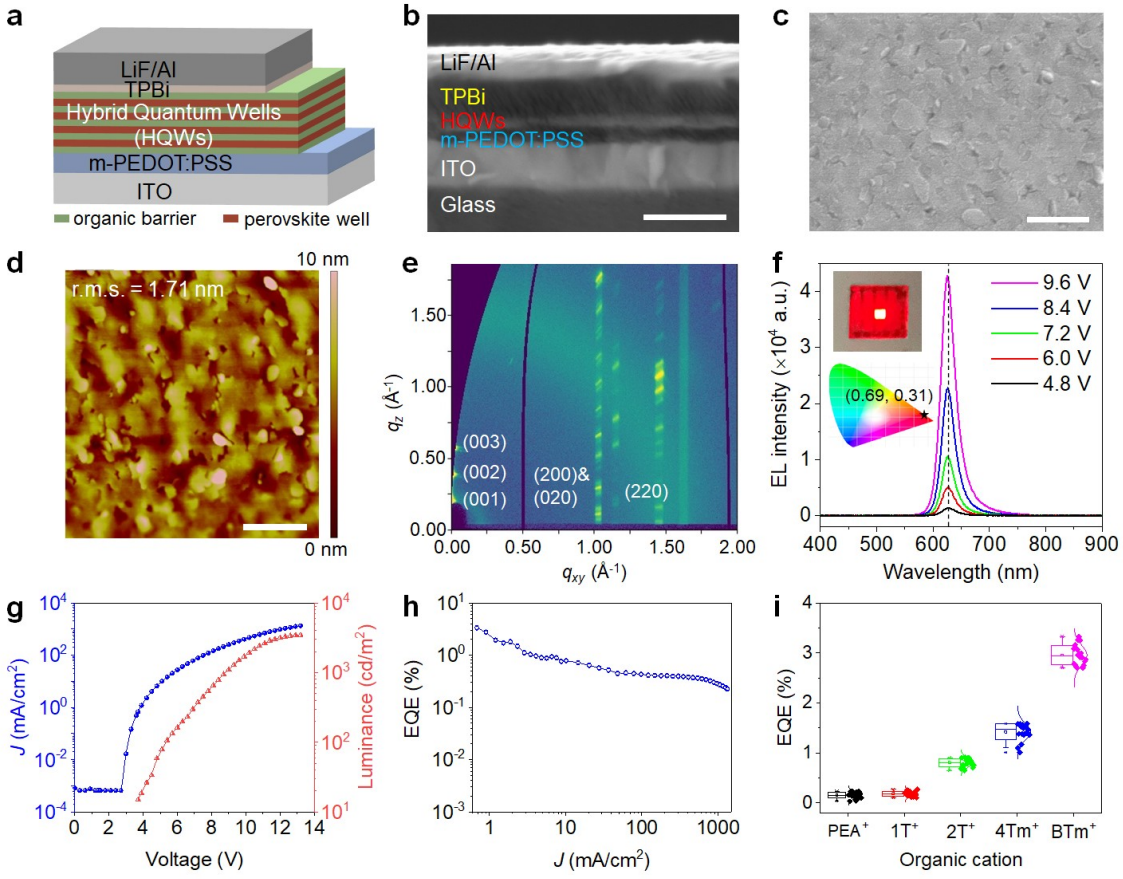

Figure 3. Structural characterizations and device performances of organic-perovskite HQW-LEDs. (a) Device structure and (b) cross-section SEM image of HQW-LED. The scale bar is 250 nm. (c - d) SEM (c) and AFM (d) images of (BTm)2SnI4 HQW layer. The scale bars are 500 nm.

(e) GIWAXS patterns for HQW thin film. (f) EL spectra under forward biases of 4.8, 6.0, 7.2, 8.4 and 9.6 V. Insets are photograph of a red-emitting device and corresponding CIE coordinate. (g - h) Current density-voltage-luminance curves (g) and EQE characteristic (h) of a champion HQW-LED device. (i) EQE distributions of 20 devices for HQW-LEDs with different organic cations, PEA^+, $1T^+$, $2T^+$, $4Tm^+$, and BTm^+.

Operational Stability. We examined the operational stability of our LED devices by measuring the luminance over time at constant current densities (Figure 4a). The $(PEA)_2SnI_4$ based HQW-LED exhibits a very short operational half lifetime (T_{50}) of ~1 min at 10 mA cm^{-2}, which is similar to the reported results.[45-47] The phenylmethylammonium iodide modified $CH_3NH_3PbI_3$ (PMAI-$MAPbI_3$) based LED has a high peak EQE of 10.1% around 10 mA cm^{-2} (Figure S14a-14c), which is consistent with that in previous literature.[56] Nevertheless, this $MAPbI_3$-based LED device also shows a limited lifetime (T_{50} = 5 min) and obvious hysteresis under forward and reverse scan (Figure S14d), suggesting significant ion migration. In contrast, our $(BTm)_2SnI_4$ based HQW-LED has a dramatically increased operational lifetime as T_{50} = 9166 min (~153 h) at 5 mA cm^{-2}, which is significantly longer than any perovskite-based red LEDs (see Video S1). Moreover, our device also shows outstanding operational stability with T_{50} of 4000 min at 10 mA cm^{-2}, 1164 min at 50 mA cm^{-2}, and 50 min at 200 mA cm^{-2}. These results can be fitted with an empirical equation, $L_0^n T_{50}$ = constant,[22] where L_0 and n are the initial luminance and acceleration factor respectively. Accordingly, n is determined to be 1.55 (Figure S15). It should be noted that the $(BTm)_2SnI_4$ HQW-LED exhibits excellent *J-V* reliability free from hysteresis under the repetition of scanning voltage between 0 and 6 V over 20 scans (Figure 4b), while the $(PEA)_2SnI_4$ HQW-LED shows non-negligible hysteresis and obvious drop of current density under repeated scans (Figure S16), which suggest greatly suppressed ion migration by the bulky and rigid

conjugated moieties,[57] accounting for this significantly higher operation stability. In addition, the $(BTm)_2SnI_4$ thin films also demonstrate better intrinsic stability than $(PEA)_2SnI_4$ counterparts regarding enhanced water stability (Figure S17) and air stability (Figure S18), which are also responsible for the remarkable operational stability. Figure 4c shows the time-dependent EL spectra, which was determined during the lifetime measurements of our $(BTm)_2SnI_4$ HQW-LED. It didn't show any wavelength shift in the EL spectra and their FWHM remained almost unchanged even after 150 hours of operation.

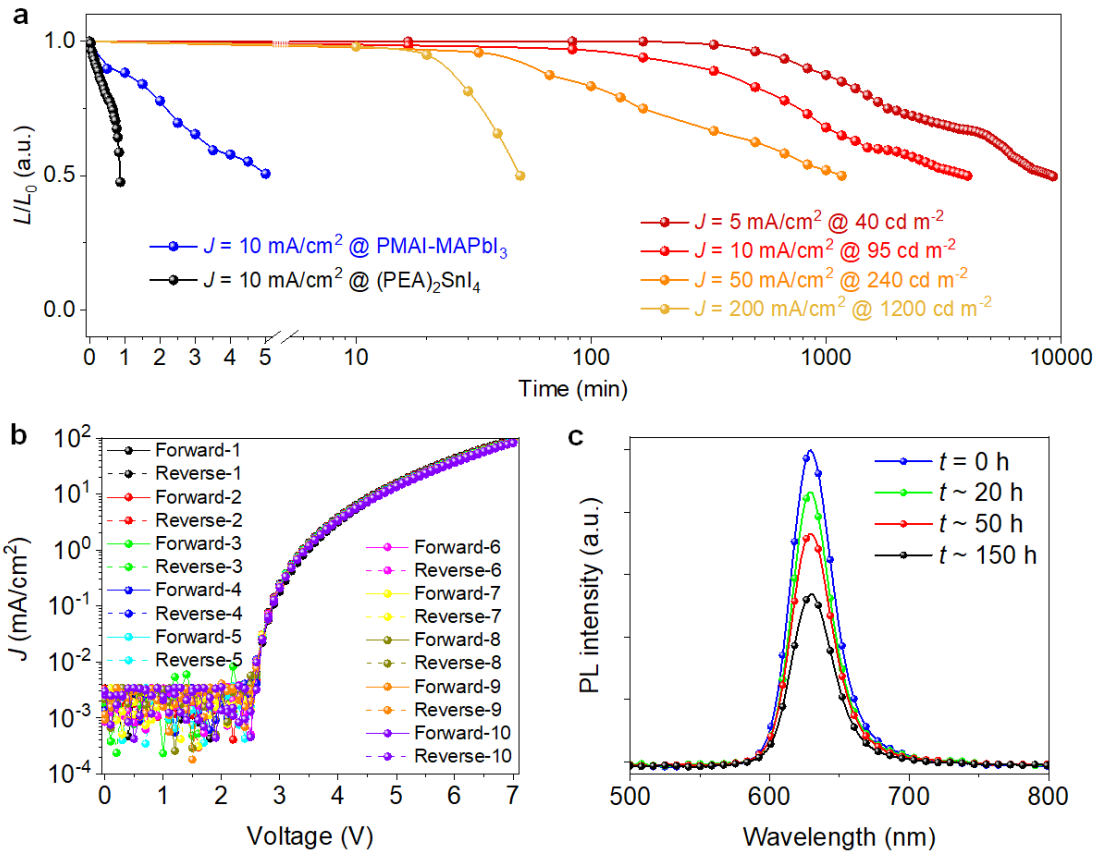

Figure 4. Device stability characterizations. (a) Operational lifetime of the hybrid perovskite LED devices for $(PEA)_2SnI_4$ (black), PMAI-$MAPbI_3$ (blue), and $(BTm)_2SnI_4$ at different current densities (from yellow, orange, red to dark red). These unencapsulated devices were tested in glove box with constant driving current densities. (b) Current density against driving voltage for

HQW-LED with different scanning directions. The scanning rate is 0.1 V/step and scanning range is 0 V to 7 V for all measurements. (c) EL spectra during operational lifetime test at 5 mA cm^{-2}, which didn't show any obvious wavelength shift after continuous lighting for about 150 hrs.

CONCLUSION

In summary, we have reported a molecular engineering approach to construct Sn-based organic-perovskite HQWs with a small barrier height. Such HQWs feature enhanced charge transport, inhibited ion migration, as well as ultrafast energy transfer, which allowed us to fabricate highly stable and efficient lead-free HQW-LEDs for the first time. More importantly, the interplay between the organic and inorganic layers is worthy of further investigation for better control and manipulation of the excitons at the organic-inorganic interface. For instance, the extremely fast energy transfer may allow the use of novel organic molecules with even smaller HOMO-LUMO gap as the barrier layer to further enhance the charge injection and transport in the out-of-plane direction. Clearly, there is a huge space for materials design and device engineering to further boost the performance. This new fundamental knowledge may lead to the discovery of highly stable lead-free non-toxic hybrid perovskite emitters for many practical applications such as LEDs, lasers, and photodetectors.

EXPERIMENTAL SECTION

Chemicals and reagents. Organic solvents, including anhydrous N,N-dimethylformide (DMF), dimethylsulfoxide (DMSO), toluene, ether, chlorobenzene (CB), dichlorobenzene (DCB), tetrahydrofuran (THF), dichloromethane (DCM), chloroform, γ-butyrolactone (GBL), lead

iodide (PbI_2), tin iodide (SnI_2, 99.99%), tin chloride ($SnCl_2$), poly(sodium 4-styrenesulfonate) (PSS-Na), hydroquinonesulfonic acid potassium salt, 1,3,5-tris(1-phenyl-1H-benzimidazol-2-yl)benzene (TPBi), LiF, and metallic tin were purchased from Sigma Aldrich. Phenethylammonium iodide (PEAI) were purchased from Greatcell Solar. All above chemicals were used as received. Other ammonium salts, including 1TI, 2TI, 4TmI and BTmI were synthesized in our lab by following the procedures reported in our previous publication[34].

Fabrication of perovskite films. A precursor solution was firstly prepared by dissolving 60 mM organic ammonium salts (such as PEAI, 1TI, 2TI, 4TmI, and BTmI), 30 mM SnI_2, 30 mM $SnCl_2$, and 1.5 mM additives (hydroquinonesulfonic acid potassium salt[55]) in DMF/DMSO (10:1 v/v) inside the nitrogen-filled glovebox. After stirring for 2 h, several centimeter-long Sn wires were dropped inside the solution, which was stirred for another hour. Then, the solution was filtered through a 0.22 μm PTFE syringe filter for further use. The substrates were treated with UVO cleaner for 30 min before transferring into a nitrogen glove-box for spin coating. The above precursor was spin-coated onto the pre-cleaned substrates at 3000 rpm for 60 s. After 15 s, 100 μL 1 mg/mL TPBi in toluene was dropped to the film, and then baked at 180 °C for 10 min. These obtained films can be used for further characterizations.

LED device fabrication. The pre-cleaned ITO substrate was treated by ultraviolet-ozone for 30 min to make the surface hydrophilic. Modified poly(3,4-ethylenedioxythiophene): poly(styrenesulfonate) (m-PEDOT:PSS) solution was prepared by mixing PEDOT:PSS solution (AI 4083) with PSS-Na aqueous solution (15 mg/mL) with a volume ratio of 1:1. Then, m-PEDOT:PSS was deposited onto ITO substrate at 3000 rpm for 35 s and baked at 150 °C for 10 min in air. Subsequently, the substrates were transferred into the glove-box followed by PEIE

deposition from 2-methoxyethanol (0.4 wt%) at 5,000 rpm for 1 min, and then annealed at 110 °C for 20 min. Next, the HQW active layers were fabricated by spin-coating the above precursors onto the PEIE surface at 3000 rpm for 60 s. Finally, TPBi (80 nm), LiF (1.2 nm) and an Al (100 nm) anode were sequentially deposited by thermal evaporation under a vacuum of <2 × 10^{-6} mbar. The active area of the devices was defined by the overlapping area of the ITO and Al electrodes.

Single-crystal growth. Single crystal growth was performed in nitrogen-filled glove box. Single crystal was obtained through a vapor diffusion method. Specifically, a 2:1 molar ratio of BTmI and SnI_2 were dissolved in GBL to make a 50 mM solution by heating at 110 ℃ for 1 h. 0.1 mL precursor solution were injected into a small vial and placed in a larger vial containing 3 mL mixed solvent of chloroform and chlorobenzene with a volume ratio of 1:2, which was immediately sealed with a cap. The system was left undisturbed for a week, yielding red to dark-red thin plates.

UV-vis absorption spectra. Thin film UV-vis spectra were taken on an Agilent UV-Vis-NIR Cary-5000 in transmission mode.

Photoluminescence (PL) spectra. Steady state PL spectra were obtained with an Olympus microscope system (BX53) integrated with an X-CITE 120Q UV lamp. The filter set contains a bandpass filter (330 - 385 nm), a dichroic mirror (cutoff wavelength, 400 nm), and a 420 nm long-pass filter. The collected PL signals were analyzed by a spectrometer (SpectraPro HRS-300).

Photoluminescence quantum yield (PLQY). The PLQY were obtained by a three-step technique with a home-designed system, which consists of a continuous-wave laser (375 nm), an integrating sphere, optical fiber and a spectrometer[58].

Scanning electron microscopy (SEM). Thin film SEM images were acquired with a Field Emission SEM (Hitachi S-4800).

Atomic force microscopy (AFM). Thin film AFM images were collected with a Bruker MultiMode 8 atomic force microscope in tapping mode.

Grazing incidence wide angle X-ray scattering (GIWAXS). GIWAXS spectra were collected at beamline 7.3.3. at the Advanced Light Source at Lawrence Berkeley National Lab utilizing an incident angel of 0.1° and wavelength of 10 keV. 2D spectra were taken with a Pilatus 2M-2D detector and integrated to reduce to 1D with the NIKA GIWAXS software. Raw data was further processed and visualized using Xi-Cam[59].

Powder XRD. HQW thin films were spin-coated on pre-cleaned glass substrates for XRD measurements. Thin film XRD was measured with a Rigaku Smart Lab (Cu Kα, λ = 1.54056 Å) in Bragg Brentano (BB) mode.

Time-resolved PL (TRPL) measurements. A home-built PL microscope was used to conduct TRPL measurements. A pulsed excitation beam (picosecond duration time, 447 nm) was generated from optical parametric amplifiers (40 MHz repetition rate). The beam was focused onto the sample by using a 40× objective (Nikon, NA = 0.6). The PL emission was collected by

the same objective, and then coupled to a single photon avalanche diode (PicoQuant, PDM series) with a single photon counting module (PicoQuant).

Transient absorption (TA) spectroscopy. Transient absorption spectra of $(BTm)_2SnI_4$ and $(PEA)_2SnI_4$ HQW thin films were measured by a home-built femtosecond pump-probe system described in a previous publication[60]. Laser pulses at 1030 nm with 250-fs pulse duration were generated by a 750 kHz amplified Yb:KGW laser system (PHAROS, Light Conversion Ltd.). By focusing part of the 1030 nm fundamental output onto a YAG crystal, the broad-band probe beam was created, spanning 450 - 950 nm spectral region. The rest of the fundamental laser was sent to an optical parametric amplifier (OPA, ORPHEUS-Twins, Light Conversion Ltd.) to generate wavelength tunable pump pulses with ~10 nm bandwidth. An optical chopper (MC200B, Thorlabs) was used to modulate the pump beam with a frequency of 195 Hz. A linear stepper motor stage (Newport) was utilized to delay the probe beam as late as 800 ps relative to the pump beam. Both pump and probe beams were focused on the sample with a 5× objective (N.A. = 0.1, Olympus). The transmission change of the probe signal was collected with a 20× objective (N.A. = 0.45, Olympus) and detected by an array detector (Exemplar LS, B&W Tek). In the pump photon energy dependent measurements, pump power has been calibrated to excite similar exciton density to allow comparison.

The TA dynamics of $(PEA)_2SnI_4$ sample was fitted by a single exponential decay function. And the TA dynamics of $(BTm)_2SnI_4$ sample with 365 nm excitation was fitted with an energy transfer model described by the rate equation:

$$\frac{\square\square_{\square}(\square\square)}{\square\square} = -\square_{\square}\square_{\square}(\square\square) - \square_{\square\square}\square_{\square}(\square\square)$$

$$\frac{dn_{Sn}(t)}{dt} = k_{ET} n_l(t) - k_{Sn1} n_{Sn}(t)$$ where k_l, k_{Sn1} are the decay rate constant of BTm^+ cation and $[SnI_4]^{2-}$ layer, respectively; k_{ET} is the energy transfer rate constant from organic cation to $[SnI_4]^{2-}$. The initial population ratio of $n_l(0)$, $n_{Sn}(0)$ was estimated to be 2:3, according to the absorption spectrum of $(PEA)_2SnI_4$ and $(BTm)_2SnI_4$ (Figure S1). k_l = 5×10^{-2} ps^{-1} was used for BTm^+ ligand in the fitting[40]. However, varying k_l from 10^{-1} to 10^{-4} ps^{-1} yields <1% change in the fitting results.

Device characterizations. All LED devices were characterized in glovebox without encapsulation. The *J-V* curves measurement were conducted on a Keithley 2450, where he devices were swept from zero bias to forward bias at a rate of 0.1 V s^{-1}. A 100 mm integrating sphere coupled with a spectrometer (Enli Technology, LQ-100X) were used for the measurements of brightness and electroluminescent spectra. The operational stabilities of such HQW-LEDs were measured at constant current densities.

ASSOCIATED CONTENT

The Supporting Information is available free of charge via the Internet at http://pubs.acs.org.

Experimental details, PLQY, TA data, SEM, AFM, LED device data, additional crystallographic data (PDF)

Crystallographic data of $(BTm)_2SnI_4$ (CIF)

Crystallographic data of $(BTm)_2PbI_4$ (CIF)

Video for over 5 hr stability (MP4)

AUTHOR INFORMATION

Corresponding Author

*__Letian Dou –__ Davidson School of Chemical Engineering, Birck Nanotechnology Center, Purdue University, West Lafayette, Indiana 47907, United States; Email: dou10@purdue.edu.

Authors

Kang Wang – Davidson School of Chemical Engineering, Purdue University, West Lafayette, IN, USA.
Linrui Jin – Department of Chemistry, Purdue University, West Lafayette, IN, USA.
Yao Gao – Davidson School of Chemical Engineering, Purdue University, West Lafayette, IN, USA.
Aihui Liang – College of Chemistry and Chemical Engineering, Jiangxi Normal University, Nanchang, China; Davidson School of Chemical Engineering, Purdue University, West Lafayette, IN, USA.
Blake P. Finkenauer – Davidson School of Chemical Engineering, Purdue University, West Lafayette, IN, USA.
Wenchao Zhao – Davidson School of Chemical Engineering, Purdue University, West Lafayette, IN, USA.
Zitang Wei – Davidson School of Chemical Engineering, Purdue University, West Lafayette, IN, USA.
Chenhui Zhu – Advanced Light Source, Lawrence Berkeley National Laboratory, Berkeley, CA, USA.
Tzung-Fang Guo – Department of Photonics, National Cheng Kung University, Tainan, Taiwan.
Libai Huang – Department of Chemistry, Purdue University, West Lafayette, IN, USA.

Author Contributions

L.D. conceived the idea and supervised the project. K.W. carried out the materials synthesis, structural characterizations, device fabrications, and data analysis. L.J. and L.H. carried out the transient absorption measurements and data analysis. Y.G. and A.L. performed organic cations

synthesis. B.F. and W.Z. performed SEM characterizations. Z.W. conducted powder XRD measurements. C.Z. carried out GIWAXS measurements. T. G. provided insightful discussions and participated data analysis and manuscript preparation. K.W. and L.D. wrote the manuscript. All authors discussed the results and revised the manuscript. ‡These authors contributed equally.

Notes

The authors declare no competing financial interest.

ACKNOWLEDGMENTS

This work is supported by Office of Naval Research (Grant No. N00014-19-1-2296, Program Manager: Dr. Paul Armistead and Dr. Joe Parker) and College of Engineering and Davidson School of Chemical Engineering of Purdue University. L.H. acknowledge the support from US Department of Energy, Office of Basic Energy Sciences through award DE-SC0016356. We thank Dr. Yuichiro Watanabe for the discussion and help with the PLQY measurements.

REFERENCES

1. Nakamura, S.; Senoh, M.; Iwasa, N.; Nagahama, S.-i., High-Brightness InGaN Blue, Green and Yellow Light-Emitting Diodes with Quantum Well Structures. *Jpn. J. Appl. Phys.* **1995,** *34*, L797-L799.

2. Qian, F.; Li, Y.; Gradečak, S.; Park, H.-G.; Dong, Y.; Ding, Y.; Wang, Z. L.; Lieber, C. M., Multi-Quantum-Well Nanowire Heterostructures for Wavelength-Controlled Lasers. *Nat. Mater.* **2008,** *7*, 701-706.

3. Hicks, L. D.; Dresselhaus, M. S., Effect of Quantum-Well Structures on the Thermoelectric Figure of Merit. *Phys. Rev. B* **1993,** *47*, 12727-12731.

4. Levine, B. F., Quantum-well infrared photodetectors. *J. Appl. Phys.* **1993,** *74*, R1-R81.

5. Ishihara, T.; Takahashi, J.; Goto, T., Exciton state in two-dimensional perovskite semiconductor $(C_{10}H_{21}NH_3)_2PbI_4$. *Solid State Commun.* **1989,** *69*, 933-936.

6. Mitzi, D. B.; Feild, C. A.; Harrison, W. T. A.; Guloy, A. M., Conducting tin halides with a layered organic-based perovskite structure. *Nature* **1994,** *369*, 467-469.

7. Dou, L.; Wong, A. B.; Yu, Y.; Lai, M.; Kornienko, N.; Eaton, S. W.; Fu, A.; Bischak, C. G.; Ma, J.; Ding, T.; Ginsberg, N. S.; Wang, L.-W.; Alivisatos, A. P.; Yang, P., Atomically thin two-dimensional organic-inorganic hybrid perovskites. *Science* **2015,** *349*, 1518-1521.

8. Weidman, M. C.; Seitz, M.; Stranks, S. D.; Tisdale, W. A., Highly Tunable Colloidal Perovskite Nanoplatelets through Variable Cation, Metal, and Halide Composition. *ACS Nano* **2016,** *10*, 7830-7839.

9. Ha, S.-T.; Shen, C.; Zhang, J.; Xiong, Q., Laser cooling of organic–inorganic lead halide perovskites. *Nat. Photon.* **2016,** *10*, 115-121.

10. Stoumpos, C. C.; Cao, D. H.; Clark, D. J.; Young, J.; Rondinelli, J. M.; Jang, J. I.; Hupp, J. T.; Kanatzidis, M. G., Ruddlesden–Popper Hybrid Lead Iodide Perovskite 2D Homologous Semiconductors. *Chem. Mater.* **2016,** *28*, 2852-2867.

11. Leng, K.; Abdelwahab, I.; Verzhbitskiy, I.; Telychko, M.; Chu, L.; Fu, W.; Chi, X.; Guo, N.; Chen, Z.; Chen, Z.; Zhang, C.; Xu, Q.-H.; Lu, J.; Chhowalla, M.; Eda, G.; Loh, K. P., Molecularly thin two-dimensional hybrid perovskites with tunable optoelectronic properties due to reversible surface relaxation. *Nat. Mater.* **2018,** *17*, 908-914.

12. Smith, M. D.; Connor, B. A.; Karunadasa, H. I., Tuning the Luminescence of Layered Halide Perovskites. *Chem. Rev.* **2019,** *119*, 3104-3139.

13. Gong, X.; Voznyy, O.; Jain, A.; Liu, W.; Sabatini, R.; Piontkowski, Z.; Walters, G.; Bappi, G.; Nokhrin, S.; Bushuyev, O.; Yuan, M.; Comin, R.; McCamant, D.; Kelley, S. O.; Sargent, E. H., Electron–phonon interaction in efficient perovskite blue emitters. *Nat. Mater.* **2018,** *17*, 550-556.

14. Kumar, S.; Jagielski, J.; Yakunin, S.; Rice, P.; Chiu, Y.-C.; Wang, M.; Nedelcu, G.; Kim, Y.; Lin, S.; Santos, E. J. G.; Kovalenko, M. V.; Shih, C.-J., Efficient Blue Electroluminescence Using Quantum-Confined Two-Dimensional Perovskites. *ACS Nano* **2016,** *10*, 9720-9729.

15. Liang, D.; Peng, Y.; Fu, Y.; Shearer, M. J.; Zhang, J.; Zhai, J.; Zhang, Y.; Hamers, R. J.; Andrew, T. L.; Jin, S., Color-Pure Violet-Light-Emitting Diodes Based on Layered Lead Halide Perovskite Nanoplates. *ACS Nano* **2016,** *10*, 6897-6904.

16. Deng, W.; Jin, X.; Lv, Y.; Zhang, X.; Zhang, X.; Jie, J., 2D Ruddlesden–Popper Perovskite Nanoplate Based Deep-Blue Light-Emitting Diodes for Light Communication. *Adv. Funct. Mater.* **2019,** *29*, 1903861.

17. Chen, H.; Lin, J.; Kang, J.; Kong, Q.; Lu, D.; Kang, J.; Lai, M.; Quan, L. N.; Lin, Z.; Jin, J.; Wang, L.-w.; Toney, M. F.; Yang, P., Structural and spectral dynamics of single-crystalline Ruddlesden-Popper phase halide perovskite blue light-emitting diodes. *Sci. Adv.* **2020,** *6*, eaay4045.

18. Cortecchia, D.; Mróz, W.; Neutzner, S.; Borzda, T.; Folpini, G.; Brescia, R.; Petrozza, A., Defect Engineering in 2D Perovskite by Mn(II) Doping for Light-Emitting Applications. *Chem* **2019,** *5*, 2146-2158.

19. Tan, Z.-K.; Moghaddam, R. S.; Lai, M. L.; Docampo, P.; Higler, R.; Deschler, F.; Price, M.; Sadhanala, A.; Pazos, L. M.; Credgington, D.; Hanusch, F.; Bein, T.; Snaith, H. J.; Friend, R. H., Bright light-emitting diodes based on organometal halide perovskite. *Nat. Nanotechnol.* **2014,** *9*, 687.

20. Cho, H.; Jeong, S.-H.; Park, M.-H.; Kim, Y.-H.; Wolf, C.; Lee, C.-L.; Heo, J. H.; Sadhanala, A.; Myoung, N.; Yoo, S.; Im, S. H.; Friend, R. H.; Lee, T.-W., Overcoming the electroluminescence efficiency limitations of perovskite light-emitting diodes. *Science* **2015,** *350*, 1222-1225.

21. Xiao, Z.; Kerner, R. A.; Zhao, L.; Tran, N. L.; Lee, K. M.; Koh, T.-W.; Scholes, G. D.; Rand, B. P., Efficient perovskite light-emitting diodes featuring nanometre-sized crystallites. *Nat. Photon.* **2017,** *11*, 108.

22. Lin, K.; Xing, J.; Quan, L. N.; de Arquer, F. P. G.; Gong, X.; Lu, J.; Xie, L.; Zhao, W.; Zhang, D.; Yan, C.; Li, W.; Liu, X.; Lu, Y.; Kirman, J.; Sargent, E. H.; Xiong, Q.; Wei, Z., Perovskite light-emitting diodes with external quantum efficiency exceeding 20 per cent. *Nature* **2018,** *562*, 245-248.

23. Cao, Y.; Wang, N.; Tian, H.; Guo, J.; Wei, Y.; Chen, H.; Miao, Y.; Zou, W.; Pan, K.; He, Y.; Cao, H.; Ke, Y.; Xu, M.; Wang, Y.; Yang, M.; Du, K.; Fu, Z.; Kong, D.; Dai, D.; Jin, Y.; Li,

G.; Li, H.; Peng, Q.; Wang, J.; Huang, W., Perovskite light-emitting diodes based on spontaneously formed submicrometre-scale structures. *Nature* **2018,** *562*, 249-253.

24. Xu, W.; Hu, Q.; Bai, S.; Bao, C.; Miao, Y.; Yuan, Z.; Borzda, T.; Barker, A. J.; Tyukalova, E.; Hu, Z.; Kawecki, M.; Wang, H.; Yan, Z.; Liu, X.; Shi, X.; Uvdal, K.; Fahlman, M.; Zhang, W.; Duchamp, M.; Liu, J.-M.; Petrozza, A.; Wang, J.; Liu, L.-M.; Huang, W.; Gao, F., Rational molecular passivation for high-performance perovskite light-emitting diodes. *Nat. Photon.* **2019,** *13*, 418-424.

25. Yuan, M.; Quan, L. N.; Comin, R.; Walters, G.; Sabatini, R.; Voznyy, O.; Hoogland, S.; Zhao, Y.; Beauregard, E. M.; Kanjanaboos, P.; Lu, Z.; Kim, D. H.; Sargent, E. H., Perovskite energy funnels for efficient light-emitting diodes. *Nat. Nanotechnol.* **2016,** *11*, 872.

26. Wang, N.; Cheng, L.; Ge, R.; Zhang, S.; Miao, Y.; Zou, W.; Yi, C.; Sun, Y.; Cao, Y.; Yang, R.; Wei, Y.; Guo, Q.; Ke, Y.; Yu, M.; Jin, Y.; Liu, Y.; Ding, Q.; Di, D.; Yang, L.; Xing, G.; Tian, H.; Jin, C.; Gao, F.; Friend, R. H.; Wang, J.; Huang, W., Perovskite light-emitting diodes based on solution-processed self-organized multiple quantum wells. *Nat. Photon.* **2016,** *10*, 699.

27. Zhao, B.; Bai, S.; Kim, V.; Lamboll, R.; Shivanna, R.; Auras, F.; Richter, J. M.; Yang, L.; Dai, L.; Alsari, M.; She, X.-J.; Liang, L.; Zhang, J.; Lilliu, S.; Gao, P.; Snaith, H. J.; Wang, J.; Greenham, N. C.; Friend, R. H.; Di, D., High-efficiency perovskite–polymer bulk heterostructure light-emitting diodes. *Nat. Photon.* **2018,** *12*, 783-789.

28. Ban, M.; Zou, Y.; Rivett, J. P. H.; Yang, Y.; Thomas, T. H.; Tan, Y.; Song, T.; Gao, X.; Credgington, D.; Deschler, F.; Sirringhaus, H.; Sun, B., Solution-processed perovskite light emitting diodes with efficiency exceeding 15% through additive-controlled nanostructure tailoring. *Nat. Commun.* **2018,** *9*, 3892.

29. Yang, X.; Zhang, X.; Deng, J.; Chu, Z.; Jiang, Q.; Meng, J.; Wang, P.; Zhang, L.; Yin, Z.; You, J., Efficient green light-emitting diodes based on quasi-two-dimensional composition and phase engineered perovskite with surface passivation. *Nat. Commun.* **2018,** *9*, 570.

30. Liu, Y.; Cui, J.; Du, K.; Tian, H.; He, Z.; Zhou, Q.; Yang, Z.; Deng, Y.; Chen, D.; Zuo, X.; Ren, Y.; Wang, L.; Zhu, H.; Zhao, B.; Di, D.; Wang, J.; Friend, R. H.; Jin, Y., Efficient blue light-emitting diodes based on quantum-confined bromide perovskite nanostructures. *Nat. Photon.* **2019,** *13*, 760-764.

31. Qin, C.; Matsushima, T.; Potscavage, W. J.; Sandanayaka, A. S. D.; Leyden, M. R.; Bencheikh, F.; Goushi, K.; Mathevet, F.; Heinrich, B.; Yumoto, G.; Kanemitsu, Y.; Adachi, C., Triplet management for efficient perovskite light-emitting diodes. *Nat. Photon.* **2019,** *14*, 70-75.

32. Wang, Q.; Wang, X.; Yang, Z.; Zhou, N.; Deng, Y.; Zhao, J.; Xiao, X.; Rudd, P.; Moran, A.; Yan, Y.; Huang, J., Efficient sky-blue perovskite light-emitting diodes via photoluminescence enhancement. *Nat. Commun.* **2019,** *10*, 5633.

33. Li, Z.; Chen, Z.; Yang, Y.; Xue, Q.; Yip, H.-L.; Cao, Y., Modulation of recombination zone position for quasi-two-dimensional blue perovskite light-emitting diodes with efficiency exceeding 5%. *Nat. Commun.* **2019,** *10*, 1027.

34. Gao, Y.; Shi, E.; Deng, S.; Shiring, S. B.; Snaider, J. M.; Liang, C.; Yuan, B.; Song, R.; Janke, S. M.; Liebman-Peláez, A.; Yoo, P.; Zeller, M.; Boudouris, B. W.; Liao, P.; Zhu, C.; Blum, V.; Yu, Y.; Savoie, B. M.; Huang, L.; Dou, L., Molecular engineering of organic–inorganic hybrid perovskites quantum wells. *Nat. Chem.* **2019,** *11*, 1151-1157.

35. Shi, E.; Yuan, B.; Shiring, S. B.; Gao, Y.; Akriti; Guo, Y.; Su, C.; Lai, M.; Yang, P.; Kong, J.; Savoie, B. M.; Yu, Y.; Dou, L., Two-dimensional halide perovskite lateral epitaxial heterostructures. *Nature* **2020,** *580*, 614-620.

36. Wang, H.; Kosasih, F. U.; Yu, H.; Zheng, G.; Zhang, J.; Pozina, G.; Liu, Y.; Bao, C.; Hu, Z.; Liu, X.; Kobera, L.; Abbrent, S.; Brus, J.; Jin, Y.; Fahlman, M.; Friend, R. H.; Ducati, C.; Liu, X.-K.; Gao, F., Perovskite-molecule composite thin films for efficient and stable light-emitting diodes. *Nat. Commun.* **2020,** *11*, 891.

37. Wang, H.; Zhang, X.; Wu, Q.; Cao, F.; Yang, D.; Shang, Y.; Ning, Z.; Zhang, W.; Zheng, W.; Yan, Y.; Kershaw, S. V.; Zhang, L.; Rogach, A. L.; Yang, X., Trifluoroacetate induced small-grained $CsPbBr_3$ perovskite films result in efficient and stable light-emitting devices. *Nat. Commun.* **2019,** *10*, 665.

38. Gao, Y.; Wei, Z.; Yoo, P.; Shi, E.; Zeller, M.; Zhu, C.; Liao, P.; Dou, L., Highly Stable Lead-Free Perovskite Field-Effect Transistors Incorporating Linear π-Conjugated Organic Ligands. *J. Am. Chem. Soc.* **2019,** *141*, 15577-15585.

39. Li, W.; Pan, Y.; Xiao, R.; Peng, Q.; Zhang, S.; Ma, D.; Li, F.; Shen, F.; Wang, Y.; Yang, B.; Ma, Y., Employing ~100% Excitons in OLEDs by Utilizing a Fluorescent Molecule with Hybridized Local and Charge-Transfer Excited State. *Adv. Funct. Mater.* **2014,** *24*, 1609-1614.

40. Song, H.; Wang, K.; Kuang, Z.; Zhao, Y. S.; Guo, Q.; Xia, A., Solvent modulated excited state processes of push–pull molecule with hybridized local excitation and intramolecular charge transfer character. *Phys. Chem. Chem. Phys.* **2019,** *21*, 3894-3902.

41. Zuo, C.; Ding, L., Modified PEDOT Layer Makes a 1.52 V V_{oc} for Perovskite/PCBM Solar Cells. *Adv. Energy Mater.* **2017,** *7*, 1601193.

42. Chiba, T.; Hayashi, Y.; Ebe, H.; Hoshi, K.; Sato, J.; Sato, S.; Pu, Y.-J.; Ohisa, S.; Kido, J., Anion-exchange red perovskite quantum dots with ammonium iodine salts for highly efficient light-emitting devices. *Nat. Photon.* **2018,** *12*, 681-687.

43. Lanzetta, L.; Marin-Beloqui, J. M.; Sanchez-Molina, I.; Ding, D.; Haque, S. A., Two-Dimensional Organic Tin Halide Perovskites with Tunable Visible Emission and Their Use in Light-Emitting Devices. *ACS Energy Lett.* **2017,** *2*, 1662-1668.

44. Zhang, X.; Wang, C.; Zhang, Y.; Zhang, X.; Wang, S.; Lu, M.; Cui, H.; Kershaw, S. V.; Yu, W. W.; Rogach, A. L., Bright Orange Electroluminescence from Lead-Free Two-Dimensional Perovskites. *ACS Energy Lett.* **2019,** *4*, 242-248.

45. Gao, C.; Jiang, Y.; Sun, C.; Han, J.; He, T.; Huang, Y.; Yao, K.; Han, M.; Wang, X.; Wang, Y.; Gao, Y.; Liu, Y.; Yuan, M.; Liang, H., Multifunctional Naphthol Sulfonic Salt Incorporated in Lead-Free 2D Tin Halide Perovskite for Red Light-Emitting Diodes. *ACS Photonics* **2020,** *7*, 1915-1922.

46. Liang, H.; Yuan, F.; Johnston, A.; Gao, C.; Choubisa, H.; Gao, Y.; Wang, Y.-K.; Sagar, L. K.; Sun, B.; Li, P.; Bappi, G.; Chen, B.; Li, J.; Wang, Y.; Dong, Y.; Ma, D.; Gao, Y.; Liu, Y.; Yuan, M.; Saidaminov, M. I.; Hoogland, S.; Lu, Z.-H.; Sargent, E. H., High Color Purity Lead-Free Perovskite Light-Emitting Diodes via Sn Stabilization. *Adv. Sci.* **2020,** *7*, 1903213.

47. Wang, Z.; Wang, F.; Zhao, B.; Qu, S.; Hayat, T.; Alsaedi, A.; Sui, L.; Yuan, K.; Zhang, J.; Wei, Z.; Tan, Z. a., Efficient Two-Dimensional Tin Halide Perovskite Light-Emitting Diodes via a Spacer Cation Substitution Strategy. *J. Phys. Chem. Lett.* **2020,** *11*, 1120-1127.

48. Liao, Y.; Shang, Y.; Wei, Q.; Wang, H.; Ning, Z., Two-dimensional tin perovskite nanoplate for pure red light-emitting diodes. *J. Phys. D: Appl. Phys.* **2020,** *53*, 414005.

49. Yuan, F.; Zheng, X.; Johnston, A.; Wang, Y.-K.; Zhou, C.; Dong, Y.; Chen, B.; Chen, H.; Fan, J. Z.; Sharma, G.; Li, P.; Gao, Y.; Voznyy, O.; Kung, H.-T.; Lu, Z.-H.; Bakr, O. M.;

Sargent, E. H., Color-pure red light-emitting diodes based on two-dimensional lead-free perovskites. *Sci. Adv.* **2020,** *6*, eabb0253.

50. Passarelli, J. V.; Fairfield, D. J.; Sather, N. A.; Hendricks, M. P.; Sai, H.; Stern, C. L.; Stupp, S. I., Enhanced Out-of-Plane Conductivity and Photovoltaic Performance in n = 1 Layered Perovskites through Organic Cation Design. *J. Am. Chem. Soc.* **2018,** *140*, 7313-7323.

51. Liu, X.-K.; Xu, W.; Bai, S.; Jin, Y.; Wang, J.; Friend, R. H.; Gao, F., Metal halide perovskites for light-emitting diodes. *Nat. Mater.* **2021,** *20*, 10-21.

52. Liang, A.; Wang, K.; Gao, Y.; Finkenauer, B. P.; Zhu, C.; Jin, L.; Huang, L.; Dou, L., Highly Efficient Halide Perovskite Light-Emitting Diodes via Molecular Passivation. *Angew. Chem. Int. Ed.* **2021**, DOI: 10.1002/anie.202100243.

53. Liu, X.; Wang, Y.; Wu, T.; He, X.; Meng, X.; Barbaud, J.; Chen, H.; Segawa, H.; Yang, X.; Han, L., Efficient and stable tin perovskite solar cells enabled by amorphous-polycrystalline structure. *Nat. Commun.* **2020,** *11*, 2678.

54. Lin, R.; Xiao, K.; Qin, Z.; Han, Q.; Zhang, C.; Wei, M.; Saidaminov, M. I.; Gao, Y.; Xu, J.; Xiao, M.; Li, A.; Zhu, J.; Sargent, E. H.; Tan, H., Monolithic all-perovskite tandem solar cells with 24.8% efficiency exploiting comproportionation to suppress Sn(II) oxidation in precursor ink. *Nature Energy* **2019,** *4*, 864-873.

55. Tai, Q.; Guo, X.; Tang, G.; You, P.; Ng, T.-W.; Shen, D.; Cao, J.; Liu, C.-K.; Wang, N.; Zhu, Y.; Lee, C.-S.; Yan, F., Antioxidant Grain Passivation for Air-Stable Tin-Based Perovskite Solar Cells. *Angew. Chem. Int. Ed.* **2019,** *58*, 806-810.

56. Xiao, Z.; Kerner, R. A.; Tran, N.; Zhao, L.; Scholes, G. D.; Rand, B. P., Engineering Perovskite Nanocrystal Surface Termination for Light-Emitting Diodes with External Quantum Efficiency Exceeding 15%. *Adv. Funct. Mater.* **2019,** *29*, 1807284.

57. Akriti; Shi, E.; Shiring, S. B.; Yang, J.; Atencio-Martinez, C. L.; Yuan, B.; Hu, X.; Gao, Y.; Finkenauer, B. P.; Pistone, A. J.; Yu, Y.; Liao, P.; Savoie, B. M.; Dou, L., Layer-by-layer anionic diffusion in two-dimensional halide perovskite vertical heterostructures. *Nat. Nanotechnol.* **2021**, DOI: 10.1038/s41565-021-00848-w.

58. de Mello, J. C.; Wittmann, H. F.; Friend, R. H., An improved experimental determination of external photoluminescence quantum efficiency. *Adv. Mater.* **1997,** *9*, 230-232.

59. Pandolfi, R. J.; Allan, D. B.; Arenholz, E.; Barroso-Luque, L.; Campbell, S. I.; Caswell, T. A.; Blair, A.; De Carlo, F.; Fackler, S.; Fournier, A. P.; Freychet, G.; Fukuto, M.; Gursoy, D.; Jiang, Z.; Krishnan, H.; Kumar, D.; Kline, R. J.; Li, R.; Liman, C.; Marchesini, S.; Mehta, A.; N'Diaye, A. T.; Parkinson, D. Y.; Parks, H.; Pellouchoud, L. A.; Perciano, T.; Ren, F.; Sahoo, S.; Strzalka, J.; Sunday, D.; Tassone, C. J.; Ushizima, D.; Venkatakrishnan, S.; Yager, K. G.; Zwart, P.; Sethian, J. A.; Hexemer, A., Xi-cam: a versatile interface for data visualization and analysis. *J. Synchrotron Radiat.* **2018,** *25*, 1261-1270.

60. Guo, Z.; Wan, Y.; Yang, M.; Snaider, J.; Zhu, K.; Huang, L., Long-range hot-carrier transport in hybrid perovskites visualized by ultrafast microscopy. *Science* **2017,** *356*, 59.

TOC:

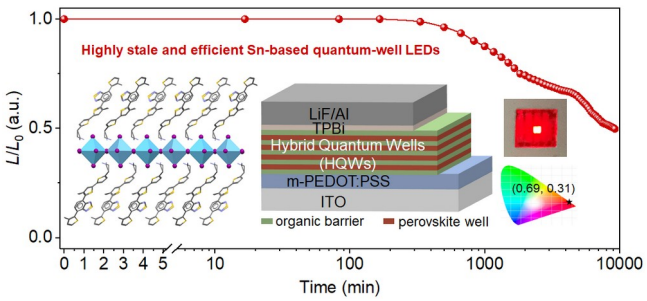
Highly stale and efficient Sn-based quantum-well LEDs
LiF/Al
TPBi
Hybrid Quantum Wells
(HQWs)
m-PEDOT:PSS
ITO
organic barrier
perovskite well
(0.69, 0.31)
L/L0 (a.u.)
1.0
0.5
0.0
0 1 2 3 4 5 10 100 1000 10000
Time (min)